ACS OMEGA

Open Access

http://pubs.acs.org/journal/acsodf

Article

Facile Synthesis of Selenium Nanoparticles for Enhanced Oxygen Evolution Reaction: Insights into Electrochemical and Photoelectrochemical Catalysis

Sumaya Ishtiaq, Ghulam Hussain, Hafiza Komal Zafar, Rabia Liaquat, Shahid Rasul, Abdullah A. Al-Kahtani, Ayman Nafady,* and Manzar Sohail*

Cite This: *ACS Omega* 2025, 10, 520−528

Read Online

ACCESS | Metrics & More | Article Recommendations | Supporting Information

ABSTRACT: Implementing a hydrogen economy on an industrial scale poses challenges, particularly in developing cost-effective and stable catalysts for water electrolysis. This study explores the catalytic potential of selenium nanoparticles (Se-NPs) synthesized via a simple chemical bath deposition method for electrochemical and photoelectrochemical (PEC) water splitting. The successful fabrication of Se-NPs on fluorine-doped tin oxide (FTO) electrodes has been confirmed using a wide range of analytical tools like X-ray diffraction, energy-dispersive X-ray spectroscopy, and scanning electron microscopy. Importantly, electrochemical measurements revealed superior electrocatalytic activity of the modified Se-NPs/FTO electrodes, with low overpotential (220 mV at 10 mA cm^{-2}) and Tafel slope (90.13 mV dec^{-1}), indicating faster reaction kinetics and reduced energy inputs for oxygen evolution reaction. Furthermore, the Se-NPs/FTO electrode was employed for PEC water splitting in Na_2S electrolyte, showing a notable enhancement in photocurrent density with a difference of 700 μA cm^{-2} between light and dark conditions at 1.5 V vs RHE, demonstrating efficient light-driven hydrogen production. The overall findings of this work establish that the proposed Se-NPs/FTO electrodes are promising composites for both electrochemical and PEC performance, thereby providing insights into developing cost-effective catalysts for large-scale water splitting.

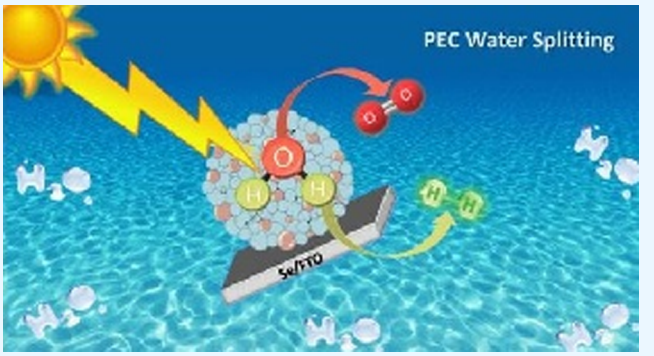

1. INTRODUCTION

The ever-increasing energy demands of a rapidly expanding global population have raised environmental concerns, particularly regarding the extensive utilization of fossil fuels and their detrimental impact on global warming.[1,2] In response to this pressing challenge, hydrogen has emerged as a pivotal eco-friendly and renewable energy source due to its zero carbon emission and potential for superior energy density approaching 142 MJ kg^{-1}[3,4] The transition toward hydrogen as a primary energy source represents a paradigm shift in the global energy landscape, offering a pathway toward decarbonization and environmental sustainability.

Scientists are actively exploring electrochemical and photoelectrochemical (PEC) water-splitting methodologies for producing hydrogen and oxygen to address environmental concerns and facilitate the transition toward sustainable energy solutions. These methodologies offer promising alternatives to conventional fuels and involve the hydrogen evolution reaction[5] (HER) on the cathode side and the oxygen evolution reaction (OER) on the anode side. The energy needed to produce 1 mol of hydrogen and 1/2 mol of oxygen from 1 mol of water is 237.2 kJ mol^{-1} at 298 K, corresponding to a potential of 1.23 V vs RHE.[6,7] The following equations show the two half-reactions on the respective electrodes.[8,9]

$$\text{(anode)} \quad 2H_2O(l) \leftrightarrow O_2(g) + 4H^+(aq) + 4e^- \quad E^\circ = +1.23\ V \tag{1}$$

$$\text{(cathode)} \quad 2H^+(aq) + 2e^- \leftrightarrow H_2(g) \quad E^\circ = 0.00\ V \tag{2}$$

Advances in water splitting have focused on integrating photoactive materials into electrode surfaces to enhance the direct conversion of solar energy into chemical energy, making hydrogen production more sustainable and efficient. This approach shows great promise for improving the efficiency of hydrogen generation through photo electrocatalysis.[1,10] Noble metals such as platinum (Pt) and iridium/ruthenium (Ir/Ru)

Received: July 31, 2024
Revised: November 26, 2024
Accepted: December 2, 2024
Published: December 26, 2024

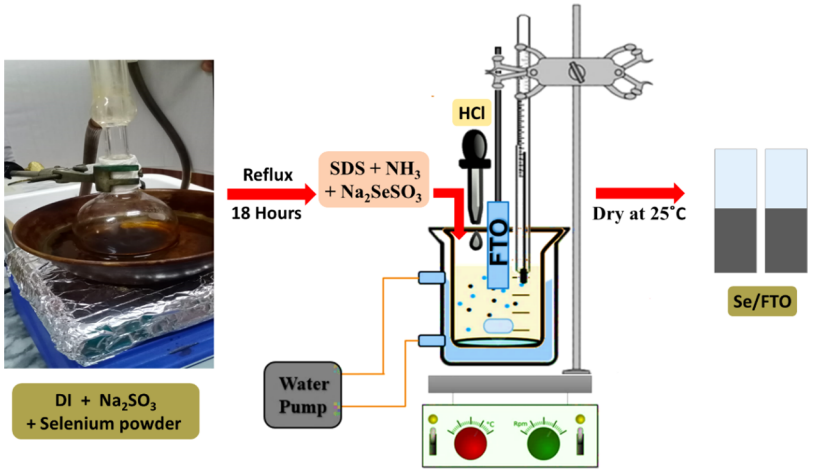

Figure 1. Schematic diagram representing the Se-NPs/FTO electrode fabrication through the CBD method.

are highly effective catalysts for HER and OER, with attributes such as high exchange current density, lower Tafel slope, and reduced overpotential. However, their finite availability and elevated costs present significant barriers to their widespread adoption. Efforts to establish a hydrogen economy on an industrial scale face challenges, particularly in developing cost-effective catalysts with prolonged stability for water electrolysis.[11−13]

To overcome challenges in developing efficient electrocatalysts, researchers are exploring alternative catalysts, particularly transition metal-based compounds such as perovskites, carbides, nitrides, and chalcogenides.[14−18] These materials offer high intrinsic electrical conductivity and favorable free energy for ion adsorption and desorption. Significant advancements have been made in the development of electrocatalysts for both HER and OER. For example, Mo_2N/Ni_3Mo_3N electrocatalysts exhibit exceptional HER activity with low overpotentials and long-term stability,[19] while transition metal oxides like $NiMoO_4$ have been optimized to enhance OER performance through strategic electronic structure modulation.[20] Chalcogenides, particularly, have emerged as critical materials for electrochemical (EC) and photoelectrochemical (PEC) water splitting due to their excellent electronic properties and stability. Transition metal chalcogenides, such as indium sulfide (In_2S_3), have shown promise in enhancing catalytic activity. Recent studies demonstrated that high-temperature flame treatment of In_2S_3 can effectively convert its surface into a diffusion-less In_2O_3 layer and generate bulk sulfur vacancies. This surface reconstruction reduces charge recombination, significantly improving photocurrent density and stability. The optimized photoanode achieved a photocurrent density of 8.5 mA cm^{-2} at 1.23 V RHE and 7.3 mA cm^{-2} at 0.6 V vsRHE for iodide oxidation reaction.[21] These advancements highlight the potential of chalcogenides in advancing PEC and EC water splitting technologies, offering promising pathways for developing efficient and cost-effective photoelectrodes. Among the transition metal chalcogenides (TMCs), selenium (Se)-based materials have shown great potential in enhancing OER activity due to their excellent semiconducting properties and high electrical conductivity.[2,10,22−25] Selenium, which is approximately 20 times more conductive than sulfur, has gained attention for its application in various electronic and photovoltaic devices.[26,27] Recent research highlights the potential of selenium in driving the water-splitting process due to its outstanding semiconducting properties and ability to undergo various valence state changes.[28−32]

In this study, selenium nanoparticles were deposited on fluorine-doped tin oxide (FTO) glass using a chemical bath deposition (CBD) method to produce a Se/FTO photocatalyst. The synthesized Se/FTO was explicitly evaluated for its OER performance in both electrochemical and PEC water splitting, and its results were compared with bare FTO glass. Our findings demonstrate that Se/FTO is a promising candidate as a photoelectrocatalyst to enhance water-splitting efficiency. This work aims to provide insights into selenium's catalytic capabilities, expanding the understanding of its photo- and electrocatalytic properties, and advancing its potential application in sustainable water-splitting technologies.

2. EXPERIMENTAL DETAILS

2.1. Materials Required. Se-powder (100 mesh, ≥99.5%), Na_2SO_3 (≥98%), sodium dodecyl sulfate (≥99.0%), HCl (37%), ammonia solution (28−30%), KOH (≥85%), and ethanol (≥99.9%), purchased from Sigma-Aldrich. All solutions were prepared using DI water from the Milli-Q system (Model: EQ-7000, from Merck KGaA, Darmstadt 64297, Germany). The FTO glass (1 × 1 cm^2) was purchased from Sigma-Aldrich.

2.2. Se/FTO Fabrication by CBD Method. The Se/FTO composite was synthesized using the CBD method described in our previous work.[25] Se-powder (2 g, 25.32 mmol) and Na_2SO_3 (6 g, 47.60 mmol) were mixed in 100 mL of DI water and refluxed for 18 h, followed by cooling and filtration to get 0.2 M sodium selenosulfate (Na_2SeSO_3) solution. The CBD apparatus involved a double-jacketed beaker, with the temperature maintained at 70 °C using circulated hot water. Freshly prepared Na_2SeSO_3 (10 mL), 20 mL of NH_3 solution, and 20 mg of sodium dodecyl sulfate (SDS) were added and stirred mechanically. The pH of the resulting CBD bath was maintained at 8.0 by gradually adding the HCl solution dropwise. Before starting the Se/FTO composite deposition, the FTO glass underwent cleaning by sonicating in ethanol and DI water for 10−15 min, then dried for 15 min at 100 °C. After cleaning the impurities, the FTO glass was suspended in the plating bath for 3 h. The resulting Se-nanoparticle-coated FTO (Se/FTO) was then removed from the reaction mixture, washed with DI water and ethanol, and dried at room

https://doi.org/10.1021/acsomega.4c07016
ACS Omega 2025, 10, 520−528

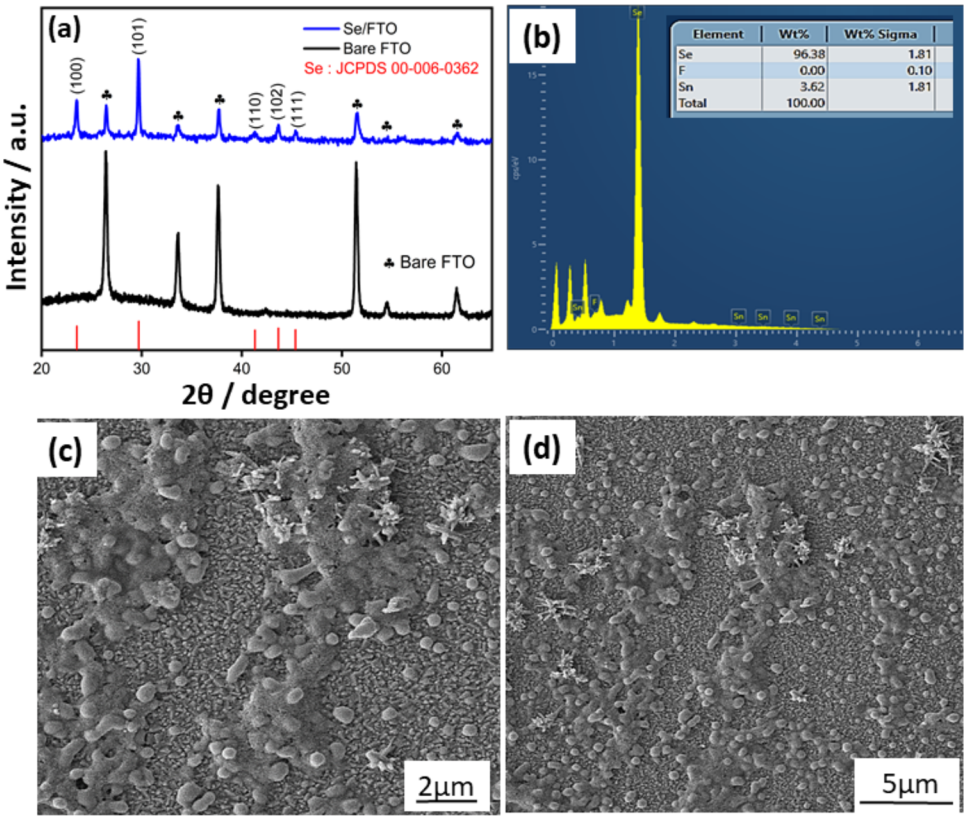

Figure 2. (a) pXRD patterns of bare FTO with the Se-NPs/FTO electrode, and (b) EDS patterns of the Se-NPs/FTO electrode and SEM images at (c) 2 μm (d) 5 μm resolutions.

temperature. The entire process is illustrated in Figure 1. Furthermore, Se-NPs in the mixture underwent washing and drying for subsequent analysis. The formation process of Se-NPs using the CBD method is explained by eqs 3 and 4.

$$2Na_2SeSO_3 + 2HCl \rightarrow 2NaCl + H_2SeSO_3 \quad (3)$$

$$H_2SeSO_3 \rightarrow Se_{nano} + SO_2 + H_2O \quad (4)$$

2.3. Structural Characterization. The crystal structures of Se nanoparticles and Se nanoparticles deposited on FTO were investigated using a DRON-8 X-ray diffractometer from Bourevestnik (Saint-Petersburg 197350, Russia) with a Cu Kα radiation source (λ = 0.15418 nm). SEM images were captured using a Nova Nano scanning electron microscope (Hillsboro, 97123, USA) at an accelerating voltage of 20 kV. The as-prepared electrode was analyzed using energy-dispersive X-ray spectroscopy (EDX) with the same Nova Nano SEM model.

2.4. Electrochemical and PEC Measurements. All electrochemical and PEC experiments were performed using a Gamry Interface potentiostat (1000E, Louis Drive, Warminster, USA) in a conventional three-electrode system. The Se-NPs/FTO coated glass was employed as the working electrode, with a Pt-wire as the counter electrode and Ag/AgCl as the reference electrode. Different electrochemical techniques such as linear sweep voltammetry (LSV), cyclic voltammetry (CV), chronoamperometry,[33] and electrochemical impedance spectroscopy[34] were used to evaluate the performance of Se-NPs/FTO compared to bare FTO glass. The EIS was conducted over the 100 000 to 0.1 Hz frequency range with an AC potential of 10 mV. All EC experiments were conducted in 1 M KOH solution as an electrolyte at room temperature. For PEC measurements, 0.1 M Na_2S solution was used as an electrolyte. All PEC measurements were conducted under an Xe lamp with a 100 mW cm^{-2} intensity.

3. RESULTS AND DISCUSSION

3.1. Structural and Morphological Study of Se-NPs/FTO. The successful deposition of Se on the surface of FTO was confirmed with powder X-ray diffraction (p-XRD). This powerful technique offers valuable insights into the atomic arrangement of crystalline substances, as depicted in Figure 2(a). The observed XRD peaks at approximately 23.5, 29.7, 41.4, 43.7, and 45.4° aligned with (100), (101), (110), (102), and (111) hexagonal planes of selenium (JCPDS# 00-006-0362).[25] Additionally, peaks appearing around 26.46, 33.64, 37.705, 51.50, 54.49, and 61.49° are the characteristic peaks of FTO and matched with the p-XRD patterns of bare FTO (Figure 1A). Furthermore, Figure 2(b) illustrates the EDS spectrum of the Se-NPs/FTO electrode, providing insights into its elemental composition where the appeared peaks correspond to selenium (Se), tin,[35] and iron (Fe), with weight percentages of 96.38, 3.25, and 0.37%, respectively, confirm the successful deposition of Se-NPs on the FTO surface.

The synthesized Se-NPs showed a distinctive globular morphology, as evidenced by SEM images in Figure 2(c,d). These nanospheres exhibited well-defined and uniform spherical structures, indicating the controlled synthesis process employed in fabricating Se-NPs/FTO. The rounded configuration of Se nanoparticles highlights the precision of their formation and emphasizes their potential significance in electrocatalytic applications. This morphology contributes to an increased surface area and enhanced electrocatalytic activity,

https://doi.org/10.1021/acsomega.4c07016
ACS Omega 2025, 10, 520−528

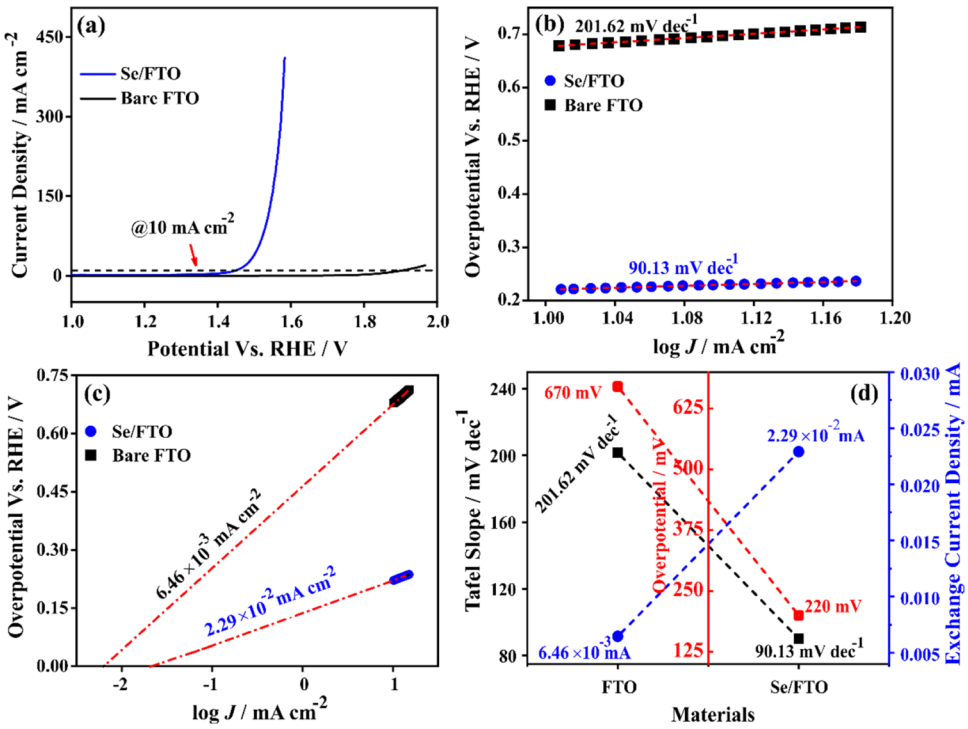

Figure 3. (a) LSV polarization curves, (b) Tafel slopes, (c) exchange current density of bare FTO and Se-NPs/FTO, and (d) a comparison of overpotential, Tafel slope, and exchange current density.

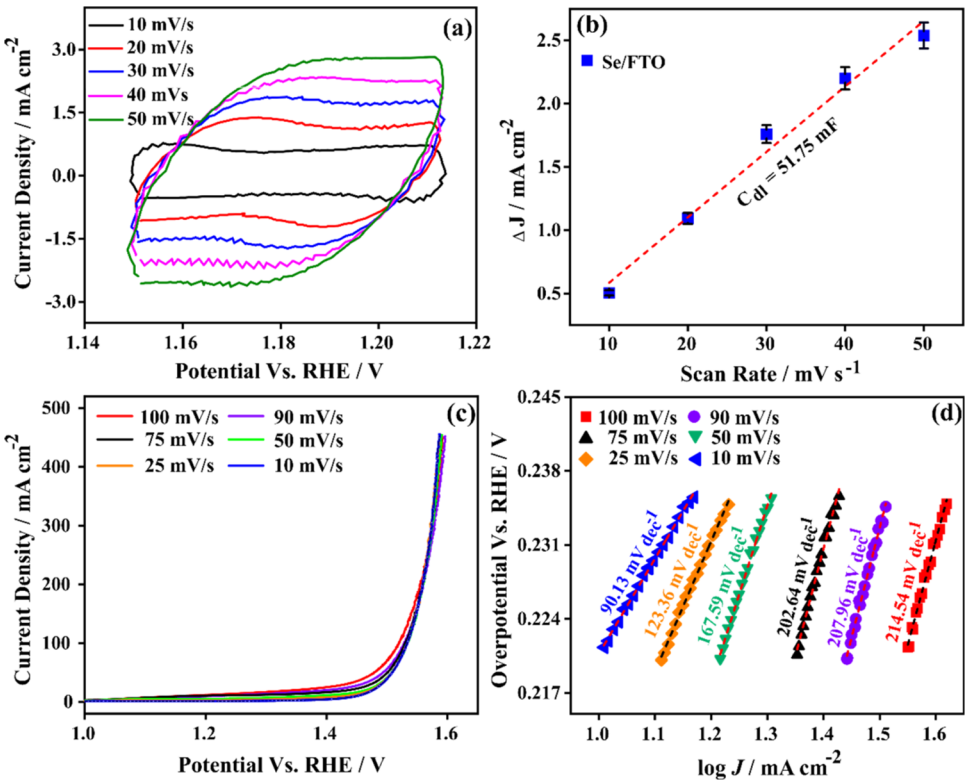

Figure 4. (a) CV polarization curves at the scan rate of 10−50 mV s^{-1} in the nonfaradaic region, (b) the calculated electrochemical double-layer capacitance (EDLC), (c) LSV polarization curves at various scan rates (10−100 mV s^{-1}), and (d) Tafel plots of the Se-NPs/FTO electrode.

further extending the performance of the Se-NPs/FTO electrode in catalyzing oxygen evolution reactions.

3.2. Electrocatalytic Activity of SE-NPS/FTO Electrode. The electrocatalytic activity of Se-NPs/FTO for OER was determined by measuring the LSV curves in 1 M KOH at the scan rate of 10 mV s^{-1} within the potential range of 1−2 V vs RHE. The LSV polarization curves shown in Figure 3(a) illustrate the performance of both bare FTO and Se-NPs/FTO electrodes. The Se-NPs/FTO electrode shows excellent performance for OER with an overpotential of 220 mV

https://doi.org/10.1021/acsomega.4c07016
ACS Omega 2025, 10, 520−528

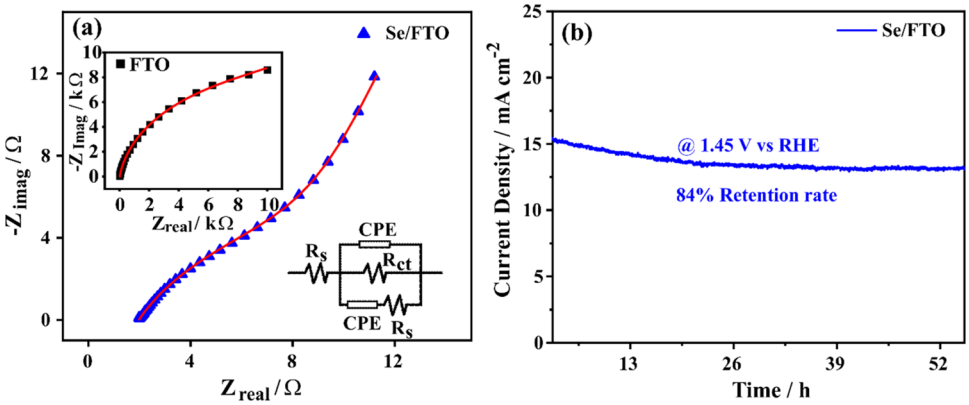

Figure 5. (a) Nyquist plot of Se-NPs/FTO electrode obtained in 1 M KOH with insets showing the Nyquist plot of bare FTO and the corresponding fitted equivalent Randles circuit. (b) Chronoamperometric stability test of Se-NPs/FTO for 52 h @ 1.45 V vs RHE.

compared to the 670 mV observed for bare FTO at 10 mA cm^{-2}. Furthermore, the Se-NPs/FTO exhibits a significantly lower Tafel slope value (90.13 mV dec^{-1}) in comparison to the bare FTO (201.62 mV dec^{-1}), providing further evidence of the enhanced reaction kinetics of Se-NPs/FTO toward the OER (Figure 3(b)).[33] The readiness of the as-synthesized electrode surface for the electrochemical OER was confirmed by evaluating the exchange current density. This was accomplished by extrapolating the Tafel plot to determine the current at zero overpotential.[36,37] The higher exchange current density value (2.29×10^{-2} mA cm^{-2}) for Se-NPs/FTO, in comparison to 6.46×10^{-3} mA cm^{-2} for bare FTO, confirms that the deposition of selenium has activated the surface of the FTO electrode (Figure 3(c)). Figure 3(d) compares overpotential, Tafel slope, and exchange current density in a single graph.

To assess the modified electrode's selectivity, cyclic voltammetry was conducted in 1 M KOH electrolyte on both bare FTO and Se-NPs/FTO electrodes between the potential range of 0.8−1.9 V vs RHE at the scan rate of 100 mV s^{-1}, as shown in SI Figure 1. The peaks observed during the positive sweep correspond to water oxidation peaks at the electrode's surface, confirming the selectivity of as-prepared electrodes for electrocatalytic OER.

The excellent electrochemical performance of Se-NPs/FTO toward OER was further confirmed by measuring the electrochemical surface area (ECSA). The ECSA was determined from the CV curves obtained at different scan rates (10−50 mV s^{-1}). These CV curves were scanned in nonfaradic regions with no substantial increase in current density, specifically within the voltage range of 0.1−0.2 V vs RHE (Figure 4(a)). The current difference (ΔJ) between the anode and cathode was plotted against the scan rate,[38,39] producing an electrochemical double-layer capacitance (C_{dl}) of approximately 51.75 mF, as shown in Figure 4(b). The resulting ECSA calculated from the SI eq (1) was 1293.75 cm^2.

The turnover frequency (TOF) is an additional activity parameter calculated at an overpotential of 220 and 670 mV with the corresponding current density of 10 mA cm^{-2} using SI eq (2).[40,41] The TOF values for Se-NPs/FTO and bare FTO were determined to be 0.1314 and 0.3693 s^{-1}, respectively, further confirming the superior electrocatalytic OER performance of the Se-NPs/FTO electrode. Figure 4(c) illustrates the LSV polarization curves of Se-NPs/FTO at various scan rates (10−100 mV s^{-1}) while maintaining the potential window from 1.0−1.6 V vs RHE. By increasing scan rates, both the overpotential and corresponding Tafel slope values increased due to the increase in double-layer charging and self-oxidation of the catalyst.[36] The Tafel slope values increase from 90.13 mV dec^{-1} at the scan rate of 10 mV s^{-1} to 214.54 mV dec^{-1} at the scan rate of 100 mV s^{-1} (Figure 4(d)).

3.3. Electrochemical Impedance Spectroscopy. The bare FTO and Se-NPs/FTO electrodes were employed for EIS analysis to evaluate the charge transfer properties at the electrode−electrolyte interface. Figure 5(a) shows the Nyquist plots of the Se-NPs/FTO electrode, and the inset shows the Nyquist plot of bare FTO for comparison. The obtained data were analyzed using a modified Randles equivalent circuit (inset of Figure 5(a)), in which R_{ct}, R_s, and CPE represent the charge transfer resistance (R_{ct}), solution resistance,[39] and constant-phase element (CPE) associated with double-layer capacitance, respectively. The smaller semicircle in the Nyquist plot of the Se-NPs/FTO electrode indicates reduced resistance compared to bare FTO, showing the superior electrochemical activity of the Se-NPs/FTO electrode. Moreover, the reduced diameter of the semicircle in the Se-NPs/FTO electrode indicates enhanced interfacial charge transfer and improved diffusion of charge carriers, resulting in minimal resistance at the electrode−electrolyte interface.[10] The charge transfer resistance and solution resistance values for Se-NPs/FTO were determined to be 7.87 and 1.83 Ω, respectively, significantly lower than the corresponding values of 12.74 and 0.48 kΩ for the bare FTO electrode (Table S1).

Stability is another essential parameter to ensure the prolonged and efficient performance of the electrochemical device. The Se-NPs/FTO electrode demonstrated excellent stability, retaining 84% of its electrocatalytic performance after continuous evaluation for 52 h, as depicted in Figure 5(b). This extended stability is crucial as it ensures the catalyst's consistent functionality over time, making it reliable for real-world applications. The excellent stability of Se-NPs over bare FTO enhances its suitability for sustainable and continuous application in real-world scenarios. A comparison of as-synthesized Se-NPs/FTO catalyst with other chalcogenide electrocatalysts is provided in SI Table 2.

3.4. Photoelectrocatalytic Activity. The PEC performance of Se-NPs/FTO was also investigated for photo water-splitting, exploring its efficiency in harnessing solar energy for hydrogen generation. In the PEC cell setup, Se-NPs/FTO was used as a photoanode, Pt wire as a cathode, and Ag/AgCl as a reference electrode. The experiment was carried out at a sweep rate of 10 mV s^{-1} in Na_2S electrolyte (0.1 M). Figure 6(a)

https://doi.org/10.1021/acsomega.4c07016
ACS Omega 2025, 10, 520−528

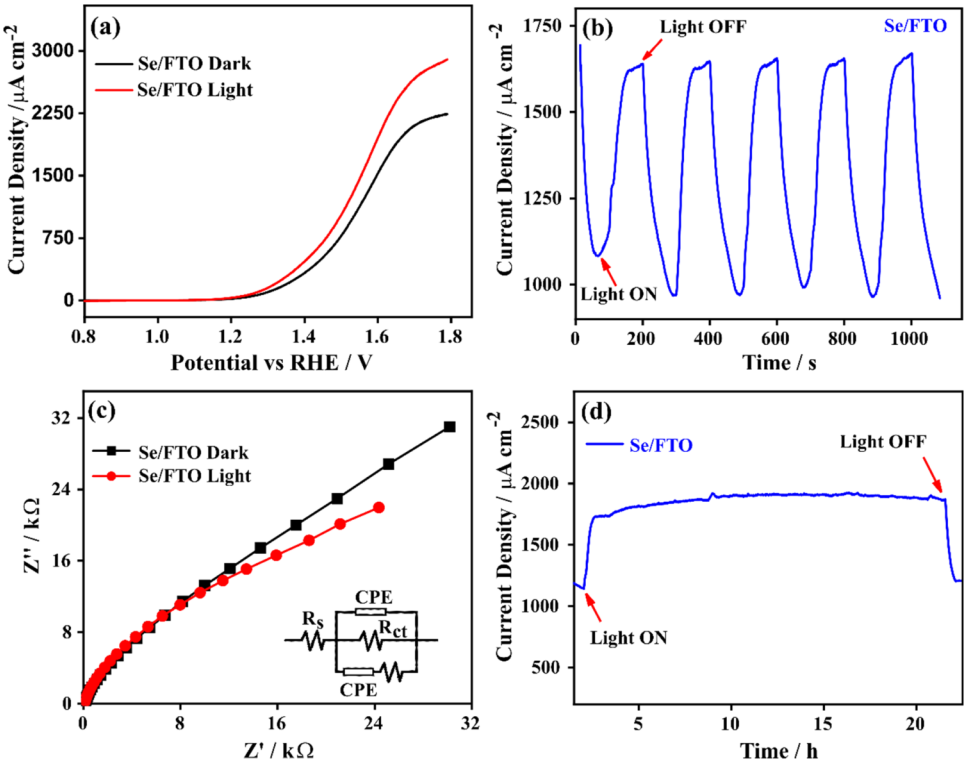

Figure 6. (a) LSV plot of Se-NPs/FTO electrode under both dark and light conditions. (b) Chronoamperometric chopping response during on/off illumination cycles after every 100 s @ 1.5 V vs RHE. (c) EIS Nyquist plots of Se-NPs/FTO under both light and dark conditions. (d) Stability of Se-NPs/FTO under light exposure for 20 h at 1.5 V vs RHE.

shows the LSV curves of the Se-NPs/FTO electrode under both dark and light conditions. The current density experiences a significant rise when the electrode is exposed to light. Specifically, the Se-NPs/FTO electrode demonstrates a current density of 2900 μA cm^{-2} in light compared to 2240 μA cm^{-2} in the dark condition. Therefore, there is a notable difference in current density of 660 μA cm^{-2} at 1.78 V vs RHE. The enhanced current density (ca. 30% increase) observed under light conditions can be attributed to the efficient photo conversion capabilities of Se-NPs/FTO, facilitated by its semiconductor properties and tailored nanostructures on the FTO substrate, improving the charge separation and migration under light illumination.[10] Consequently, this enhancement significantly improves the overall PEC performance of Se-NPs/FTO, making it a promising candidate for efficient hydrogen generation in PEC cells.

Figure 6(b) depicts the chronoamperometric chopping response of Se-NPs/FTO, demonstrating the variations in photocurrent during 100 s intervals of off/on illumination cycles at 1.5 V. The gradual decrease and subsequent increase in photocurrent upon turning off and on the light indicate a slow recombination rate. Specifically, when the light is turned off, the current decreases from 1660 to 960 μA cm^{-2}, resulting in a photocurrent difference of 700 μA cm^{-2} at 1.5 V vs RHE. This observation highlights that Se-NPs/FTO maintains stable and efficient charge separation, contributing to its good performance in PEC applications.

Figure 6(c) shows electrochemical impedance spectroscopy,[34] presenting distinctive semicircles in Nyquist plots with noticeable variations in size under both light and dark conditions. The smaller semicircle observed under light conditions indicates lower resistance in the Se-NPs/FTO electrode, signifying enhanced charge transfer kinetics and efficient electron transport during PEC reactions. In contrast, the larger semicircle observed in the dark suggests higher resistance, implying decreased electron mobility and hindered charge transfer processes. Interpreting EIS in both light and dark conditions provides valuable insights into the behavior of the Se-NPs/FTO electrode. Under light, the reduced resistance signifies improved electron mobility and enhanced charge separation, contributing to superior PEC performance. The increased resistance in the dark implies decreased electron mobility, possibly due to reduced photon absorption and hindered charge transfer processes. These observations confirm the photoresponsive nature of the Se-NPs/FTO electrode and its capability to facilitate efficient charge transport during light-induced reactions.[10,42]

Stability is another important parameter that characterizes the catalyst's performance in practical applications. Figure 6(d) represents the stability evaluation of Se-NPs/FTO photocatalyst under light exposure for 20 h, demonstrating consistent performance with no noticeable decrease in photocurrent density. This stability highlights the durability of the Se-NPs/FTO electrode in maintaining PEC properties over time. The absence of degradation in photocurrent density reinforces its reliability for prolonged use, rendering it suitable for applications in sustained hydrogen production.

4. CONCLUSIONS

In this study, we investigated the potential of Se-NPs fabricated via a facile CBD method for efficient water-splitting applications, both electrochemical and PEC. Our findings shed light on the promise of Se as a catalyst in these processes, offering insights into its electrocatalytic and photoelectrocata-

https://doi.org/10.1021/acsomega.4c07016
ACS Omega 2025, 10, 520−528

lytic capabilities. We confirmed the successful synthesis of Se nanoparticles on FTO electrodes by employing different characterization techniques, including XRD, SEM, and EDX. These nanoparticles exhibited a distinct spherical morphology, contributing to their increased surface area and enhanced electrocatalytic activity. Electrochemical measurements revealed the superior performance of the Se-NPs/FTO electrodes compared to bare FTO for OER. The Se-NPs/FTO electrodes have been verified to exhibit a reduced overpotential of 220 mV at a sweep rate of 10 mA cm^{-2} with a Tafel slope measuring 90.13 mV dec^{-1}, indicating faster reaction kinetics and reduced energy inputs for OER. Moreover, the higher exchange current density (2.29×10^{-2} mA cm^{-2}), larger electrochemical surface area (ECSA, 1293.75 cm^2), and smaller value of turnover frequency (TOF, 0.1314 s^{-1}) further underscored the high electrocatalytic performance of Se-NPs/FTO electrodes in alkaline media. In PEC water splitting, Se-NPs/FTO electrodes exhibited a notable enhancement in photocurrent density (1660 μA cm^{-2}) under light conditions, showcasing their efficiency in harnessing solar energy for hydrogen generation. The observed photocurrent density difference (700 μA cm^{-2} @ 1.5 V vs RHE) between light and dark conditions highlights the potential of Se-NPs/FTO electrodes for efficient light-driven hydrogen production. Furthermore, the Se-NPs/FTO electrode exhibited remarkable stability during an extended 52 h evaluation, retaining 84% of its electrocatalytic performance. This extended stability positions the Se-NPs/FTO catalyst as a reliable and durable solution for practical applications. In short, this study offers significant findings regarding the catalytic capabilities of selenium nanoparticles synthesized via the CBD method, offering promising avenues for developing cost-effective and durable catalysts suitable for large-scale water splitting, thereby contributing to the advancement of sustainable energy solutions.

■ ASSOCIATED CONTENT

Supporting Information

The Supporting Information is available free of charge at https://pubs.acs.org/doi/10.1021/acsomega.4c07016.

CV curves of bare FTO and Se-NPs/FTO at the scan rate of 100 mV s^{-1} (Figure S1); calculations for the electrochemical surface area; turnover frequency; the calculated values of circuit elements by circuit fitting on Nyquist plots of bare FTO and Se-NPs/FTO (Table S1); the comparison of Se/FTO catalysts with other chalcogenide electrocatalysts (Table S2) (PDF)

■ AUTHOR INFORMATION

Corresponding Authors

Ayman Nafady − *Chemistry Department, College of Science, King Saud University, Riyadh 11451, Saudi Arabia*; Email: anafady@ksu.edu.sa

Manzar Sohail − *Department of Chemistry, School of Natural Sciences, National University of Sciences and Technology, Islamabad 44000, Pakistan*; orcid.org/0000-0003-1457-2491; Email: manzar.sohail@sns.nust.edu.pk

Authors

Sumaya Ishtiaq − *Department of Chemistry, School of Natural Sciences, National University of Sciences and Technology, Islamabad 44000, Pakistan*; Present Address: School of Chemistry, University of New South Wales, Sydney, New South Wales 2052, Australia

Ghulam Hussain − *Department of Chemistry, School of Natural Sciences, National University of Sciences and Technology, Islamabad 44000, Pakistan*

Hafiza Komal Zafar − *Department of Chemistry, School of Natural Sciences, National University of Sciences and Technology, Islamabad 44000, Pakistan*

Rabia Liaquat − *US-Pakistan Center for Advanced Studies in Energy, National University of Sciences and Technology, Islamabad 44000, Pakistan*

Shahid Rasul − *Faculty of Engineering and Environment, Northumbria University, Newcastle Upon Tyne NE1 8ST, U.K.*

Abdullah A. Al-Kahtani − *Chemistry Department, College of Science, King Saud University, Riyadh 11451, Saudi Arabia*

Complete contact information is available at: https://pubs.acs.org/10.1021/acsomega.4c07016

Author Contributions

S.I.: Investigation, writing—original draft, investigations. G.H.: Formal analysis, reviewing and editing. H.K.Z.: Writing—reviewing, investigation. R.L.: Formal analysis, reviewing and editing. S.R.: Writing—reviewing, resources. A.N.: Writing—review and editing, funding acquisition. A.A.Al-K.: Writing—review and editing, funding acquisition. M.S.: Conceptualization, supervision, reviewing, writing and editing, funding acquisition.

Notes

The authors declare no competing financial interest.

■ ACKNOWLEDGMENTS

The Higher Education Commission (HEC), Pakistan, supported this work through grant no. HEC-NRPU 15745. The authors extend our sincere appreciation to the Researchers Supporting Project Number (RSP2025R266) at King Saud University, Riyadh, Saudi Arabia, for partial support of this work.

■ REFERENCES

(1) Tahir, N.; Altaf, A.; Baig, N.; Nafady, A.; Ul-Hamid, A.; Shah, S. S. A.; Tsiakaras, P.; Sohail, M. Engineering Mn-Doped CdS Thin Films Through Chemical Bath Deposition for High-Performance Photoelectrochemical Water Splitting. *Chem. - Asian J.* **2024**, *19*, No. e202301100.

(2) Jo, S.; Lee, K.; Sohn, J. I. Metallic selenium as novel bifunctional electrocatalysts for highly efficient overall water electrolysis. *Appl. Surf. Sci.* **2021**, *544*, No. 148845.

(3) Zhang, B.; Zheng, Y.; Ma, T.; Yang, C.; Peng, Y.; Zhou, Z.; Zhou, M.; Li, S.; Wang, Y.; Cheng, C. Designing MOF Nanoarchitectures for Electrochemical Water Splitting. *Adv. Mater.* **2021**, *33* (17), No. 2006042.

(4) He, Y.; Hu, Y.; Zhu, Z.; Li, J.; Huang, Y.; Zhang, S.; Balogun, M. S.; Tong, Y. High-performance multidimensional-structured N-doped nickel modulated Mo2N/FeOxNy bifunctional electrocatalysts for efficient alkaline seawater splitting. *Chem. Eng. J.* **2024**, *489*, No. 151348.

(5) Wang, Y.; Seo, B.; Wang, B.; Zamel, N.; Jiao, K.; Adroher, X. C. Fundamentals, materials, and machine learning of polymer electrolyte membrane fuel cell technology. *Energy AI* **2020**, *1*, No. 100014.

(6) Hassan, A.; Komal Zafar, H.; Shahid Ashraf, R.; Arfan, M.; Rezaul Karim, M.; Wahab, M. A.; Sohail, M. Ferrocene-Boosted Nickel Sulfide Nanoarchitecture for Enhanced Alkaline Water Splitting. *Chem. - Asian J.* **2024**, *19*, No. e202301051.

(7) Maeda, K.; Domen, K. Photocatalytic Water Splitting: Recent Progress and Future Challenges. *J. Phys. Chem. Lett.* **2010**, *1* (18), 2655−2661.
(8) Chang, C.-J.; Chu, Y.-C.; Yan, H.-Y.; Liao, Y.-F.; Chen, H. M. Revealing the structural transformation of rutile RuO_2 via in situ X-ray absorption spectroscopy during the oxygen evolution reaction. *Dalton Trans.* **2019**, *48* (21), 7122−7129.
(9) Iqbal, Z.; Miran, W.; Ul-Hamid, A.; Sohail, M.; Azad, F. Tailored Flower-Like Ni-Fe-MOF-Derived oxide Composites: Highly active and durable electrocatalysts for overall water splitting. *Fuel* **2021**, *372*, No. 132112.
(10) Zafar, H. K.; Sohail, M.; Nafady, A.; Ostrikov, K. K.; Will, G.; Wahab, M. A.; O'Mullane, A. P. S-doped copper selenide thin films synthesized by chemical bath deposition for photoelectrochemical water splitting. *Appl. Surf. Sci.* **2023**, *641*, No. 158505.
(11) Park, S.; Utsch, N.; Carmo, M.; Shviro, M.; Stolten, D. Iridium−Nickel Nanoparticle-Based Aerogels for Oxygen Evolution Reaction. *ACS Appl. Nano Mater.* **2022**, *5* (12), 18060−18069.
(12) Tian, J.-W.; Fu, M.-X.; Huang, D.-D.; Wang, X.-K.; Wu, Y.-P.; Lu, J. Y.; Li, D.-S. A new 2D Co5-cluster based MOF: Crystal structure, magnetic properties and electrocatalytic hydrogen evolution reaction. *Inorg. Chem. Commun.* **2018**, *95*, 73−77.
(13) Li, Y.; Sun, Y.; Qin, Y.; Zhang, W.; Wang, L.; Luo, M.; Yang, H.; Guo, S. Recent Advances on Water-Splitting Electrocatalysis Mediated by Noble-Metal-Based Nanostructured Materials. *Adv. Energy Mater.* **2020**, *10* (11), No. 1903120.
(14) Ashraf, I.; Ahmad, S.; Rizwan, S.; Iqbal, M. Fabrication of Ti3C2@MoO3 nanocomposite as an electrode material for highly efficient and durable water splitting system. *Fuel* **2021**, *299*, No. 120928.
(15) Sivanantham, A.; Lee, H.; Hwang, S. W.; Lee, H. U.; Cho, S. B.; Ahn, B.; Cho, I. S. Complementary Functions of Vanadium in Boosting Electrocatalytic Activity of CuCoNiFeMn High-Entropy Alloy for Water Splitting. *Adv. Funct. Mater.* **2023**, *33* (34), No. 2301153.
(16) Asif, U. A.; Noor, T.; Pervaiz, E.; Iqbal, N.; Zaman, N. LSTN (La0.4Sr0.4Ti0.9Ni0.1O3-&) perovskite and graphitic carbon nitride (g-C3N4) hybrids as a bifunctional electrocatalyst for water-splitting applications. *J. Alloys Compd.* **2023**, *939*, No. 168668.
(17) Jeong, Y. J.; Seo, D. H.; Baek, Jh.; Kang, M. J.; Kim, B. N.; Kim, S.; Zheng, X.; Cho, I. S. Crystal Reconstruction of Mo:BiVO4: Improved Charge Transport for Efficient Solar Water Splitting. *Adv. Funct. Mater.* **2022**, *32* (52), No. 2208196.
(18) Cho, I. S.; Chen, Z.; Forman, A. J.; Kim, D. R.; Rao, P. M.; Jaramillo, T. F.; Zheng, X. Branched TiO2 nanorods for photoelectrochemical hydrogen production. *Nano Lett.* **2011**, *11* (11), 4978−4984.
(19) Zhu, Z.; Luo, L.; He, Y.; Mushtaq, M.; Li, J.; Yang, H.; Khanam, Z.; Qu, J.; Wang, Z.; Balogun, M. S. High-Performance Alkaline Freshwater and Seawater Hydrogen Catalysis by Sword-Head Structured Mo2N-Ni3Mo3N Tunable Interstitial Compound Electrocatalysts. *Adv. Funct. Mater.* **2024**, *34* (8), No. 2306061.
(20) Xiong, T.; Huang, B.; Wei, J.; Yao, X.; Xiao, R.; Zhu, Z.; Yang, F.; Huang, Y.; Yang, H.; Balogun, M. S. Unveiling the promotion of accelerated water dissociation kinetics on the hydrogen evolution catalysis of NiMoO4 nanorods. *J. Energy Chem.* **2022**, *67*, 805−813.
(21) Jeong, Y. J.; Tan, R.; Nam, S.; Lee, J. H.; Kim, S. K.; Lee, T. G.; Shin, S. S.; Zheng, X.; Cho, I. S. Rapid Surface Reconstruction of In2S3 Photoanode via Flame Treatment for Enhanced Photoelectrochemical Performance. *Adv. Mater.* **2024**, No. 2403164.
(22) Hu, Z.; Wu, Z.; Han, C.; He, J.; Ni, Z.; Chen, W. Two-dimensional transition metal dichalcogenides: interface and defect engineering. *Chem. Soc. Rev.* **2018**, *47* (9), 3100−3128.
(23) Chia, X.; Ambrosi, A.; Lazar, P.; Sofer, Z.; Pumera, M. Electrocatalysis of layered Group 5 metallic transition metal dichalcogenides (MX2, M = V, Nb, and Ta; X = S, Se, and Te). *J. Mater. Chem. A* **2016**, *4* (37), 14241−14253.
(24) Lee, J.; Kang, S.; Yim, K.; Kim, K. Y.; Jang, H. W.; Kang, Y.; Han, S. Hydrogen Evolution Reaction at Anion Vacancy of Two-Dimensional Transition-Metal Dichalcogenides: Ab Initio Computational Screening. *J. Phys. Chem. Lett.* **2018**, *9* (8), 2049−2055.
(25) Ishtiaq, S.; Sohail, M.; Rasul, S.; Zia, A. W.; Siller, L.; Chotana, G. A.; Sharif, M.; Nafady, A. Selenium Nanoneedles Deposited on a Pencil Graphite Electrode for Hydrazine Sensing. *ACS Appl. Nano Mater.* **2022**, *5* (10), 14336−14346.
(26) Singh, B.; Gautam, S.; Aggarwal, V.; Kumar, R.; Singh, V. N.; Kushvaha, S. S. Selenium-based Metal Chalcogenides Thin Films on Flexible Metal Foils for PEC Water-Splitting Applications. In *Nanomaterials for Energy and Sensor Applications*; CRC Press, 2024; pp 94−122.
(27) Wei, Y.; Huang, M.; Wu, Y.; Tang, X.; Yuan, K.; Chen, Y. Selenium-Based Catalysts for Efficient Electrocatalysis. *Adv. Funct. Mater.* **2024**, *34*, No. 2404787.
(28) Tabassum, J.; Baig, N.; Sohail, M.; Nafady, A.; Shah, S. S. A.; Ul-Hamid, A.; Tsiakaras, P. Novel and efficient Bi-doped CoTe nanosolar evaporators embedded on leno weave cotton gauze for efficient solar-driven desalination. *J. Colloid Interface Sci.* **2024**, *658*, 758−771.
(29) Patil, A. M.; Kumbhar, V. S.; Chodankar, N. R.; Lokhande, A. C.; Lokhande, C. D. Electrochemical behavior of chemically synthesized selenium thin film. *J. Colloid Interface Sci.* **2016**, *469*, 257−262.
(30) Chen, Y.-W.; Zhou, X.-L.; Tong, J.; Truong, Y.; Belzile, N. Photochemical behavior of inorganic and organic selenium compounds in various aqueous solutions. *Anal. Chim. Acta* **2005**, *545* (2), 149−157.
(31) Xia, X.; Wang, L.; Sui, N.; Colvin, V. L.; William, W. Y. Recent progress in transition metal selenide electrocatalysts for water splitting. *Nanoscale* **2020**, *12* (23), 12249−12262.
(32) Wang, Z.; Liu, S.; Duan, W.; Xing, Y.; Hu, Y.; Ma, Y. Transition metal selenides as catalysts for electrochemical water splitting. *Int. J. Hydrogen Energy* **2024**, *60*, 1414−1432.
(33) Wang, M.; Dang, Z.; Prato, M.; Shinde, D. V.; De Trizio, L.; Manna, L. Ni−Co−S−Se Alloy Nanocrystals: Influence of the Composition on Their in Situ Transformation and Electrocatalytic Activity for the Oxygen Evolution Reaction. *ACS Appl. Nano Mater.* **2018**, *1* (10), 5753−5762.
(34) Chen, X.; Leishman, M.; Bagnall, D.; Nasiri, N. Nanostructured gas sensors: From air quality and environmental monitoring to healthcare and medical applications. *Nanomaterials* **2021**, *11* (8), 1927.
(35) Mitić, V.; Pavlović, V.; Kocić, L.; Paunović, V.; Mančić, D. Application of the intergranular impedance model in correlating microstructure and electrical properties of doped BaTiO3. *Sci. Sintering* **2009**, *41* (3), 247−256.
(36) Anantharaj, S.; Noda, S.; Driess, M.; Menezes, P. W. The Pitfalls of Using Potentiodynamic Polarization Curves for Tafel Analysis in Electrocatalytic Water Splitting. *ACS Energy Lett.* **2021**, *6* (4), 1607−1611.
(37) Barbir, F. Chapter Three - Fuel Cell Electrochemistry. In *PEM Fuel Cells*, 2nd ed.; Barbir, F., Ed.; Academic Press: Boston, 2013; pp 33−72.
(38) Huo, X.; Zhang, H.; Shen, W.; Miao, X.; Zhang, M.; Guo, M. Bifunctional aligned hexagonal/amorphous tungsten oxide core/shell nanorod arrays with enhanced electrochromic and pseudocapacitive performance. *J. Mater. Chem. A* **2019**, *7* (28), 16867−16875.
(39) McCrory, C. C. L.; Jung, S.; Peters, J. C.; Jaramillo, T. F. Benchmarking heterogeneous electrocatalysts for the oxygen evolution reaction. *J. Am. Chem. Soc.* **2013**, *135* (45), 16977−16987.
(40) Anantharaj, S.; Ede, S. R.; Karthick, K.; Sam Sankar, S.; Sangeetha, K.; Karthik, P. E.; Kundu, S. Precision and correctness in the evaluation of electrocatalytic water splitting: revisiting activity parameters with a critical assessment. *Energy Environ. Sci.* **2018**, *11* (4), 744−771.
(41) Raveendran, A.; Chandran, M.; Dhanusuraman, R. A comprehensive review on the electrochemical parameters and recent material development of electrochemical water splitting electrocatalysts. *RSC Adv.* **2023**, *13* (6), 3843−3876.

https://doi.org/10.1021/acsomega.4c07016
ACS Omega 2025, 10, 520−528

(42) Bai, S.; Han, J.; Zhang, K.; Zhao, Y.; Luo, R.; Li, D.; Chen, A. rGO decorated semiconductor heterojunction of BiVO4/NiO to enhance PEC water splitting efficiency. *Int. J. Hydrogen Energy* **2022**, *47* (7), 4375−4385.

https://doi.org/10.1021/acsomega.4c07016
ACS Omega 2025, 10, 520−528